Materials Advances

ROYAL SOCIETY OF CHEMISTRY

PAPER

View Article Online
View Journal

Cite this: DOI: 10.1039/d5ma01493j

Surface functionalized binary antibiotic nanoparticles of enhanced antimicrobial action

Nuriya Nurlankyzy, [a] Yersin Kalmagambet, [b] Arailym Kadir, [b] Amro K. F. Dyab [b] and Vesselin N. Paunov *[b]

Bacteria develop antimicrobial resistance (AMR) much faster than the discovery and the introduction of novel antibiotic drugs, which is an intricate and costly process. A potential solution is to find novel ways of reformulating already developed antibiotics. Here we propose a formulation of binary antibiotic nanoparticles fabricated from existing antibiotics which can strongly enhance their individual antimicrobial effects. These formulations consist of mixed nanocrystals of co-precipitated anionic antibiotic (*e.g.* sodium cefoperazone) and a cationic antibiotic (*e.g.* tetracycline hydrochloride) sterically stabilized with a surface-active polymer (Poloxamer 407) and further coated with a cationic surfactant. The cationic surface functionality is aimed to enhance the electrostatic adherence of the nanoparticles to the negatively charged bacterial cell walls leading to sustained simultaneous release of high local concentration of both antibiotics. These binary antibiotic nanoparticles are based on "safer-by-design" concept and can fully dissolve with time. We explored the antimicrobial effect of binary antibiotic particles of three different surface coatings:hexadecyl trimethylammonium bromide (HDTAB), octadecyl trimethylammonium bromide (ODTAB) and dioctadecyl dimethylammonium bromide (DODAB). The antimicrobial efficacy of the cationic surface-functionalized particles was evaluated on both Gram-negative and Gram-positive bacterial strains, *Escherichia coli* and *Staphylococcus aureus*. This approach resulted in an enhanced antimicrobial effect compared to the individual application of each of the free antibiotics at equivalent overall concentration. The produced binary antibiotic nano-delivery system showed low-to-moderate cytotoxicity on human cells. This may make them potentially applicable as injectable formulations as no nanocarrier is left post use. This innovative approach for reformulating pairs of existing antibiotics seems a promising way for breathing new life into existing antibiotics.

Received 21st December 2025,
Accepted 11th March 2026

DOI: 10.1039/d5ma01493j

rsc.li/materials-advances

1. Introduction

Antibiotic resistant bacterial infections are considered as a very serious issue in post-operational therapy in hospitals and are one of the leading sources of poor patient outcomes and mortality.[1] The ability to control bacterial infections requires using safe, affordable, and commonly available antibiotics which are crucial for disruption of bacterial growth and survival. This typically involves the impairment of the synthesis of bacterial cell membranes and walls, as well as RNA, DNA, and protein synthesis.[2,32,52] As a result of widely spread antibiotic misuse, both in humans and in agriculture, AMR has emerged as one of the most significant risks to public health worldwide.[25] Increasing of antibiotic therapeutic doses in treatment of bacterial diseases, results in greater infectious resistance and, hence, appearance of highly resistant pathogenic organisms.[4] Strains with multiple resistance to antimicrobials and antibiotics such as *Klebsiella pneumoniae*, *Enterococcus faecium, Acinetobacter baumannii* and *Escherichia coli* are spreading across the world.[32,51] This allows a selection of evermore antibiotic-tolerant microbes over time: primarily through horizontal transfer and mobilization,[30,31] the acquisition of a plethora of gene mutations leading to resistance; strengthening and developing of internal resistance mechanisms: (i) efflux pumps which support an extracellular gradient reducing the concentration of the antibiotic inside the bacteria; (ii) enzymatic inactivation of the antibiotic; (iii) decreased membrane permeability; (iv) modification of the target to reduce antibiotic affinity and others.[5,26–28,32,33,52,55] Treating infections is often hindered due to the ability of certain bacteria to grow biofilms where they can effectively isolate and resist the antibiotic action.[34,41,58,59] Future approaches to tackle the AMR are likely to focus on narrow-spectrum agents and therapeutics[5] which may help to mitigate this desperate situation.[55–57] The discovery of new antimicrobials and antibiotics is lagging far behind the spread of AMR.[54]

[a] *Department of Biology, School of Sciences and Humanities, Nazarbayev University, Kabanbay Batyr Avenue 53, Astana, 010000, Kazakhstan*
[b] *Department of Chemistry, School of Sciences and Humanities, Nazarbayev University, Kabanbay Batyr Avenue 53, Astana, 010000, Kazakhstan. E-mail: vesselin.paunov@nu.edu.kz; Tel: +7(7172)709514*

There is an urgent need to develop novel antimicrobials and smart formulation strategies that can overcome AMR and provide a viable alternative to traditional antibiotic formulations.[3,32,52,58] Alternative approaches have recently been explored by development of antimicrobial nanoparticles made from metals,[6–8] metal oxides[9–11,60,62–64] and hydroxides,[61] carbon-based materials, and polymers,[10,12–15,53,65] that may either inhibit or eradicate a variety of microorganisms using different pathways for which AMR has not yet occurred. These nanomaterials are potentially viable replacement for traditional antibacterial drugs because of their distinct physicochemical features, which allow overcome AMR and boost antibiotic effectiveness.[16–18]

Antibacterial nanomaterials exhibit encouraging outcomes in preventing or eliminating pathogenic microorganisms[10,19] in a variety of applications, including wastewater purification, healing of chronic wounds, medical devices, as well as preservation and storage of food.[29,35,36] Silver based nanoparticles work by emitting Ag^+ ions that bind to the cell wall of the bacteria[20–22,65] and limit their metabolism.[37,38] $Mg(OH)_2$NPs support a zone of high pH around them which disrupts bacterial cellular membranes.[60] Others, like photocatalytic nanoparticles ZnONPs, CuONPs and TiO_2NPs when exposed to UV light, generate reactive oxygen species that may damage the cell membranes, organelles and DNA of microbial cells.[23,24,60–64] Al-Awady *et al.*,[50] Weldrick *et al.*[51] and Al-Obaidy *et al.*[14,48,66] have recently proposed innovative approaches for enhancing antimicrobial efficiency by designing active antibiotic nanocarriers based on carbomer nanogels and shellac NPs. They demonstrated that these types of functionalised nanocarriers of common antibiotics can accumulate on the bacteria cell walls and deliver high local dose of antimicrobial agent directly on their cell walls which overpowers their defences. This approach was found to work well for a range of bacteria with efflux pumps-based resistance for tetracycline, lincomycin, as well as for vancomycin, ciprofloxacin, and others. They demonstrated that these antibiotic nanocarriers have very low toxicity for human keratinocytes at concentrations where they completely deactivate the resistant bacteria. Weldrick *et al.*[15,49,58] and Wang *et al.*[59] adapted further this novel nanotechnology approach to target bacterial biofilms, based on protease-functionalized nanogel carriers of antibiotics. Such active antibiotic nanocarriers, surface coated with a protease, can "digest" their way through the biofilm EPS matrix by targeting glycoproteins, help to reach the "buried" bacteria and deliver a locally the antibiotic within the biofilm. Very high biofilm clearance has been demonstrated without adverse effect on human cell tissues. Functionalization of the nanoparticles surface can allow different interactions with the microorganism, cell wall and the extracellular polymeric substances of the biofilms. Anionic and zwitterionic nanomaterials have low extracellular biofilm penetration, while cationic nanomaterials with the proper hydrophobic structure may penetrate the biofilm matrix.[39] Particle shape also mater and rougher nanoparticles lead to more cellular injury damaging cell membrane of pathogens.[40,62,63] Despite the high antibacterial efficiency and biocompatibility, these active antibiotic nanocarriers cannot biodegrade in the body after the release of their antibiotic payload, which renders them suitable only for topical treatment of infected surface wounds.[41–44,58–64] The preparation of potentially injectable antibiotic nanocarriers requires a different approach which is "safer-by-design"[65] and allows for disintegration of the nanocarrier post-use which offers its byproducts a way out of circulation and lower toxicity.

In this study we aim to develop degradable antibiotic nanocarriers which could potentially be used as injectable treatment for sustained local delivery of antibiotic to targeted bacteria. This is achieved by developing binary antibiotic nanoparticles which completely dissolve in the media after their payload is delivered. The idea is to design a novel type of binary antibiotic nanoparticles produced by co-precipitation of cationic and anionic antibiotics (Fig. 1):

$$A^+Cl^-(aq) + Na^+B^-(aq) \rightleftharpoons A^+B^-(s) + NaCl(aq) \quad (1)$$

where A^+Cl^- and Na^+B^- are cationic and anionic antibiotics, respectively, and $A^+B^-(s)$ is a binary antibiotic salt of lower solubility produced as nanoparticles. The A^+B^-NPs particle size is controlled by the presence of a surface-active polymer (Poloxamer 407) which sterically stabilizes the particles in aqueous solution and acts as a caping agent. The produced particles are further engineered with a cationic surface functionality to be able to electrostatically adhere to bacterial cell walls. This was achieved by doping the surface of the binary antibiotic nanoparticles with a layer of cationic surfactant at very low overall concentration. We explored three different cationic surfactants, two of which are insoluble in the aqueous phase (ODTAB and DODAB). All cationic surfactants were delivered into the $A^+B^-(s)$ particle suspension as ethanolic solution where following the ethanol attrition they were deposited on the particle surface. The novelty of the developed binary antibiotic particles is threefold: (i) the bacteria would be targeted by a nanocarrier which accumulates on their cell walls and simultaneously delivers two antibiotics with different mechanisms of action, which would help to overcome their antibiotic resistance; (ii) the local antibiotic concentrations emitted by the binary antibiotic nanoparticles would be locally sustained on the bacterial cell wall at the A^+B^- salt solubility limit of until the binary nanocrystals completely dissolve; (iii) the binary antibiotic nanocarrier could be potentially applied as for oral or injectable therapy as it would completely dissolve and disintegrate after its antimicrobial action is completed, without leaving residue or causing a biodegradability issues.

Here we show that these binary antibiotic nanoparticles require lower overall concentrations of antibiotics to eradicate both Gram-positive and Gram-negative bacteria compared to free antibiotics applied individually, thus allowing to reduce the therapeutic dosage, increasing antimicrobial efficiency. Since two different antibiotics are constituting the nanocarrier, each with a distinct mechanism of action, may target better AMR mechanisms. There is a large number of combinations of cationic and anionic antibiotics which can be formulated in binary antibiotic nanoparticles using this strategy. The nanoparticles consist solely of binary antibiotic nanocrystals coated with negligible amounts of surface polymers, which means that there would be no residues left in circulation once they are fully

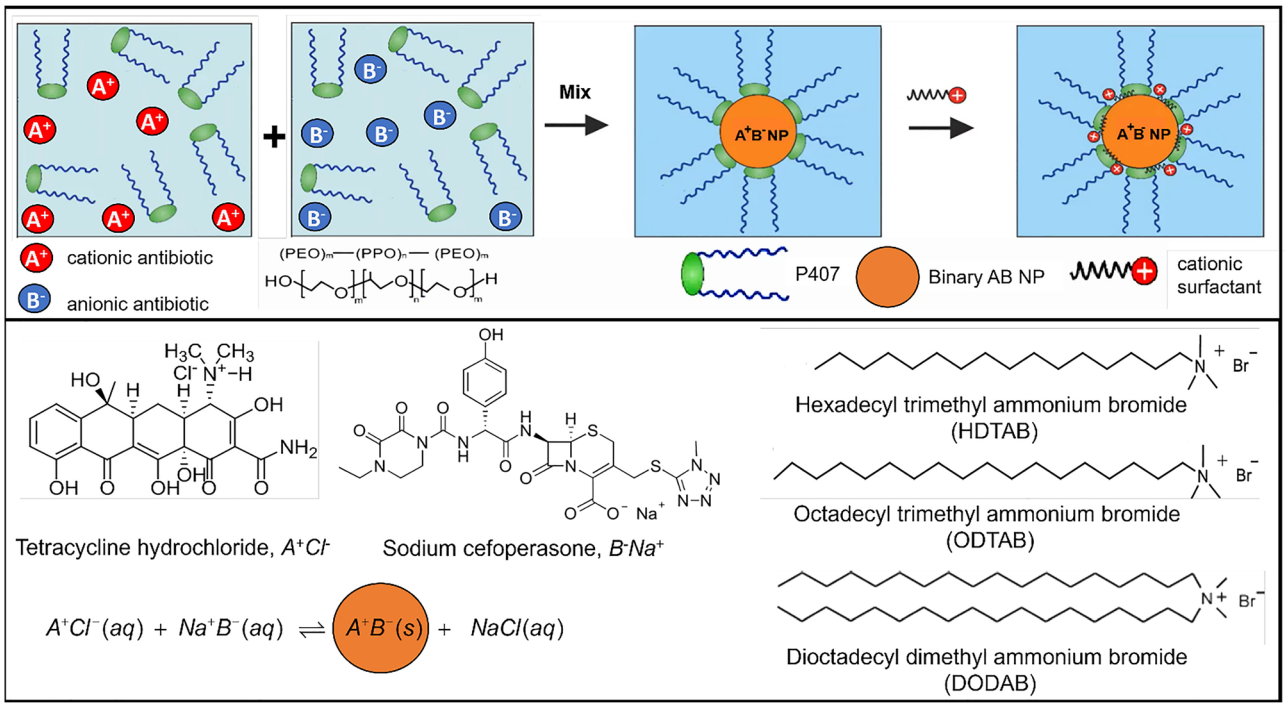

Fig. 1 Schematic presentation of the fabrication of binary antibiotic nanoparticles by co-precipitation of a cationic (A^+Cl^-) and an anionic (Na^+B^-) antibiotic aided by steric stabilisation with a surface-active polymer (Poloxamer 407) and further surface functionalised by doping with a cationic surfactant (HDTAB, ODTAB or DODAB). The cationically functionalised binary antibiotic nanoparticles can adhere electrostatically to the bacterial cell walls which are negatively charged in aqueous media. Upon dilution of the binary antibiotic nanoparticle formulation, it provides sustainable release of both antibiotics until the complete dissolution of the binary antibiotic cores. The concept is demonstrated here with two specific antibiotics, tetracycline hydrochloride and sodium cefoperazone.

depleted from antibiotics, except for negligible amounts of the sterically stabilizing polymers and the cationic surfactants from the surface coating. We also explored the cationic surfactant role in the antibacterial action and its potential cytotoxicity on human keratinocytes. This feature makes the formulation potentially promising for oral or intravenous administration. We envisage that this study is only the proof-of-concept of *in vitro* exploration of this type of binary antibiotic nanocarriers, and in the future more detailed and expanded *in vivo* studies would be needed to further explore their potential clinical effects and applications.

2. Experimental

2.1. Materials

Sodium cefoperazone (16 113, 99%) was purchased from Cayman Chemicals, Inc. and tetracycline hydrochloride (BIT0150, 99%) was delivered by Apollo Scientific, UK. Sodium hydroxide pellet (99%) and hydrochloric acid (min 36 wt%) were purchased from Thermofisher Scientific, KZ. *Staphylococcus aureus* (ATCC 23235) and *Escherichia coli* (ATCC 25922) were sourced from the American Type Culture Collection, USA. Nutrient broth & Mueller Hinton agar were supplied by Carolina, USA. Isopropanol (99+%), phosphate saline buffer (PBS, pH 7.4), trypsin/EDTA kit, Hoechst 33342 (#H1399) was sourced from Thermofisher, KZ; Dulbecco's modified Eagle's medium (DMEM F-12, #A0166-5G), acetone, (≥99.5%, #32201) and osmium tetroxide (OsO_4), #50-188-0875 were ordered from Sigma-Aldrich, KZ. (DMEM F-12 no phenol red, #21041025) and foetal bovine serum (FBS) were delivered from Gibco, UK. Poloxamer 407 (P407, M.W. 12–13 KDa, purified, #16758-250G), Propidium Iodide (PI, 99%, #P1304MP), ammonium acetate (HPLC grade), acetonitrile (HPLC grade), hexadecyltrimethylammonium bromide (HDTAB, 98%, #227160100) and dioctadecyl trimethylammonium bromide (DODAB, 98%, #408260050) were purchased from Thermofisher Scientific, KZ. Octadecyl trimethylammonium bromide (ODTAB, 98%, # BD146020) was purchased from BLD Pharm Ltd, China. Glutaraldehyde (25% aqueous solution, #111-30-8) was sourced from Avantor Science Central, UK. CellTiter 96® Aqueous One Solution Reagent™ (MTS, or (3-(4,5-dimethylthiazol-2-yl)-5-(3-carboxymethoxyphenyl)-2-(4-sulfophenyl)-2*H*-tetrazolium)) was purchased by Promega, UK. We used HaCaT cell line, (AddexBio Inc., Catalog #T0020001), a spontaneously immortalized human keratinocyte cell line from adult skin, was used as a proxy for human cells for binary antibiotic particle cytotoxicity studies. For all experiments deionized (DI) water was used purified by reverse osmosis and ion exchange with Smart2Pure system (Thermofisher Scientific, KZ) with resistivity of 18 MΩ cm^{-1}.

2.2. Methods

2.2.1. Cefoperazone and tetracycline antibiotic pair solubility determination *via* HPLC. To determine the aqueous solubility of tetracycline (Tc) and cefoperazone (Cf) as a pair in binary antibiotic co-crystals, ultra-high-performance liquid chromatography

method (UHPLC) was used. First, the standard calibration curves were obtained for each antibiotic. Samples were prepared by dissolving the individual antibiotics (tetracycline hydrochloride or sodium cefoperazone) in DI water at the following known concentrations, ranging from 0.5 ppm to 50 ppm (0.5 ppm, 1 ppm, 2.5 ppm, 5 ppm, 10 ppm, 20 ppm, 30 ppm and 50 ppm). The solutions obtained of different concentrations were filtered through 0.22 μm syringe filters to remove any undissolved antibiotic particles. By using the conditions given in Table S1 (SI), the prepared solutions were detected, and all experimental measurements were conducted *via* Dionex Ultimate 3000 HPLC with DAD. Further, to determine the solubility of the antibiotics pair, 4 mM tetracycline hydrochloride (Tc) and 4 mM cefoperazone sodium salt (Cf) solutions were prepared. For that, 19.2 mg tetracycline and 26.7 mg cefoperazone were weighed out, and each was dissolved in the 10 mL, 0.05 wt% solution of Poloxamer 407. The two separate antibiotic solutions were mixed at the same volume and left to reach an equilibrium for half an hour. The resulting mixture was centrifuged for 30 min at 70 000 g and the resulting supernatant was filtered through 0.22 μm syringe filter and injected into HPLC Hypersil Gold C18 column as a stationary phase. 20 vol% CH_3CN, 80 vol% 10 mM CH_3COONH_4 at pH 4 was used as a mobile phase. The UV-vis detector set at wavelength of 250 nm was used to calculate the concentration of each antibiotic in the supernatant after centrifugation of the nanocrystals of the binary antibiotics. The concentration of each antibiotic was then calculated by linear regression equation of the calibration curves of peak area *versus* the concentration.

2.2.2. Zeta-potential and particle size of cefoperazone and tetracycline particles stabilised by 0.05 wt% P407. The 4 mM tetracycline hydrochloride and 4 mM sodium cefoperazone solutions were prepared by dissolving 19.2 mg tetracycline and 26.7 mg cefoperazone in 10 mL 0.05 wt% aqueous solution of P407. A 2 mL aliquot of resulting 4 mM cefoperazone solution was added to 2 mL of the 4 mM tetracycline solution dropwise under 300 rpm stirring on a magnetic stirrer. The final concentration of each antibiotic in this 4 mL mixture was 2 mM. The mixture was left for 15 min to equilibrate, after which the average hydrodynamic diameter and ζ-potential measurements were performed by dynamic light scattering (DLS) and electrophoretic light scattering (ELS) using the integrated instrument Litesizer 500 (Anton Paar Austria). Solutions of concentrations 1 mM, 1.25 mM, 1.5 mM and 1.75 mM were prepared using the same protocol. The particle size distribution was recorded to determine the average nanoparticle hydrodynamic diameter, and the mean ζ-potential was measured to assess the magnitude and the sign of the surface charge of the particles. To study the stability of the particles over time, particle size and ζ-potential measurements were performed from 0 hours up to 72 hours. To study the effect of dilution on the binary antibiotic particle formulation, the particles suspensions were diluted with DI water to achieve the desired overall concentration and the DLS and ELS measurements were taken.

2.2.3. Binary antibiotic NPs preparation protocol and their surface charge reversal by coating with HDTAB or ODTAB or DODAB. In typical preparation of binary antibiotic particles used further in this study, a 1 : 1 volume ratio of 4 mM cefoperazone and 4 mM tetracycline solutions, both dissolved as solids in 0.05 wt% P407, were mixed at 20 °C and left to incubate for 30 min at constant stirring with magnetic stirrer. The produced binary antibiotic particles in this suspension were further coated with a cationic surfactant (HDTAB or ODTAB or DODAB) added as a small aliquot as 3 wt% ethanolic solution. Typically, 40 μL of HDTAB or ODTAB or 100 μL of DODAB solution were used per 4 mL of the binary antibiotic particle suspension. The particle size and ζ-potential distributions were measured by using Litesizer 500 at various time intervals, ranging from 5 min to 240 hours. To study the effect of dilution on the particle size and ζ-potential, the coated stock formulation was diluted with DI water to achieve the desired final concentration.

2.2.4. TEM images, EDS analysis and FTIR spectra. To visualize the morphological characteristics of the NPs, the TEM and SEM were utilized. For TEM imaging, the NPs were made 1 day prior to imaging *via* the methods described in Section 2.2.3. The suspensions of non-coated and coated binary antibiotic particles were centrifuged at 70 000 g for 30 min. The resulting pellets were diluted up to 200 μL and 20 μL from the diluted solution and drop-casted onto carbon-coated copper grids for TEM imaging. The grids with NPs were dried overnight and the images were obtained *via* JEOL JEM-1400 Plus TEM. To obtain SEM images, two different methods were used, and images were obtained *via* Scanning Electron Microscope ZEISS Crossbeam 540. The first one was to use a 100 nm pore membrane (nucleopore polycarbonate) to filter the NPs. The residue left on top of the pore membrane was coated with 5 nm layer of gold and platinum prior to the SEM analysis. The second method consisted of drying the obtained pellet of the centrifuged NPs overnight. The dried powder was also coated with gold/platinum layer and taken to SEM imaging.

Attenuated total reflectance Fourier transform infrared (ATR-FTIR) Spectrometer - Nicolet iS12 (ThermoFisherScientific, Germany) – was used to obtain IR spectra of the components of NPs and the NPs formulations itself. It was used to analyze the functional groups on the produced NPs. After centrifugation, the resulting pellets for the non-coated and coated binary antibiotic NPs were put and dried on filter paper and collected for FTIR recording along with the individual antibiotics (tetracycline hydrochloride and sodium cefoperazone powders), P407, HDTAB, ODTAB, DODAB powders. The spectra for all the stated powders and NPs pellets were recorded in the range of 4000 cm^{-1} to 400 cm^{-1} wavenumber, and obtained results were analyzed through Origin Lab software.

2.2.5. Antibiotic release profile for free antibiotics and binary antibiotic NPs *via* dialysis. The release profiles of free tetracycline and cefoperazone as well as the non-coated nanoparticles was be determined using a dialysis method. 20 mL 2 mM tetracycline and 20 mL 2 mM cefoperazone solutions were prepared and placed in the dialysis bags (pore size 12–14 kDa). The binary antibiotic NPs formulation made by 1 : 1 mixing of 10 mL of 4 mM tetracycline hydrochloride and 10 mL 4 mM sodium cefoperazone, both in 0.05 wt% P407 was also placed into dialysis bag double folded and sealed with clamps carefully

to prevent any leakage from the edges. The dialysis bags with 20 mL constituent each were submerged in 100 mL DI water with continuous magnetic stirring at 100 rpm. At predetermined time intervals of 5 min, 1 h, 2 h, 3 h, 6 h, 12 h, 18 h, 24 h, 38 h and 60 h, 1 mL of the release medium was withdrawn from the outside solution and replaced with equivalent aliquot of DI water to ensure the same volume of the solution in the beaker. The released antibiotic concentration from the beaker was measured by HPLC at appropriate conditions described on Table S1 (SI).

2.2.6. Antimicrobial activity of non-coated and HDTAB/ODTAB/DODAB coated binary antibiotic nanoparticles. The time-kill curves for the free antibiotics, the non-coated NPs and HDTAB-coated, ODTAB-coated, DODAB-coated binary antibiotic NPs were determined by treating *E. coli* and *S. aureus* bacteria with 6 different treatment concentrations of each condition. Before the experiment, the *E. coli* and the *S. aureus* was sub-cultured overnight in nutrient broth and adjusted to OD_{600} = 0.1 McFarland standard. Free antibiotics solutions and the non-coated and HDTAB/ODTAB/DODAB binary antibiotic NPs were tested at various concentrations ranging from 32 μM to 1 μM obtained by dispensing various aliquots of the original stock in the bacterial broth. The bacterial growth was monitored by measuring the absorbance at 600 nm (OD600) after treatment at predetermined time intervals: 0 h, 2 h, 6 h, 12 h, 18 h and 24 h to get the "time-kill" values. The viability of bacteria was also recorded in 24 h after incubating the bacterial cells for all treatment the untreated control at 37 °C.

2.2.7. SEM images of *E. coli* and *S. aureus* bacteria treated with HDTAB/ODTAB/DODAB coated binary antibiotic NPs. To obtain SEM images of *E. coli* and *S. aureus* bacteria treated with coated binary antibiotic NPs, a fixation method was used after incubation of the bacteria with the NPs treatment. After preparing all necessary HDTAB/ODTAB/DODAB-coated NPs, the bacterial broth adjusted to OD_{600} = 0.1 McFarland standard was treated with each type of these treatments and the control (no treatment, but with equivalent aliquot of DI water) and the resulting suspensions were incubated for 1.5 h in a shaking incubator at 110 rpm. After the incubation time passed, the tubes were centrifuged to obtain the pellets of bacteria with NPs. Fixation protocol included 2 h fixation of pellets in 2.5% glutaraldehyde solution in 0.1 M PBS at pH 7.4. Then, the glutaraldehyde was removed, and the pellet was washed with the same PBS buffer 3 times. Post-fixation process was done for 2 h using 1% OsO_4 in the same PBS buffer. After this, the pellets were washed 2 times in a PBS buffer and DI water, and the resulting pellets were dried on the surface of a clean glass slide (5 mm × 5 mm) overnight at room temperature. SEM imaging was done after 5 nm gold coating using Scanning Electron Microscope ZEISS Crossbeam 540.

2.2.8. Cytotoxicity of the coated and non-coated binary antibiotic particle formulations as well as their constituents on HaCaT cells. HaCaT cells were used to assess the cytotoxicity of the used nanoparticle formulations. The cells were cultured in DMEM F-12 with 10% FBS and 1% L-glutamine in T75 flasks with humidified conditions at 37 °C and 5% CO_2 until they achieved 80% confluency, as assessed with a brightfield microscopy. After achieving 80% confluency, the old culture medium was aspirated from the cells, and the flask was washed with PBS. Then 1× trypsin EDTA was used to detach the cells from the flask. To achieve full detachment, the flask was placed in an incubator for 20–30 minutes at 37 °C and 5% CO_2. After trypsinization, the trypsin was neutralized by addition of complete media (DMEM : FBS 90 : 10), and the resultant cells were resuspended and placed into a 15 mL Falcon tube. The cell suspension was centrifuged at 400 rpm for 5 min and the supernatant was aspirated. The remaining cells pellet was resuspended in a certain amount of fresh DMEM. The cells were counted using Cellometer X2 (Nexelom Biosciences Ltd, UK) and appropriate calculations were made to seed 7000 HaCaT cells per well, in 100 μL volume, in a 96-well plate. The cells were incubated for 24 h at 37 °C and 5% CO_2 incubator. After 24 h, the culture media was aspirated and fresh DMEM F-12 media was added to each well. Free antibiotics, NPs constituents, non-coated binary NPs and HDTAB/ODTAB/DODAB-coated binary antibiotic NPs were prepared freshly and HaCaT cells were treated with 32 μM concentration of each condition (with respect to the antibiotics or P407). The HaCaT cells were incubated with each treatment for another 24 h. Then the old culture media was removed from the wells and fresh DMEM F-12 with no Phenol Red was added to the wells. 10 μL CellTiter 96® Aqueous One Solution Reagent TM (Promega, UK) was added to each well and the plate was incubated for 2 h to 3 h. The absorbance was measured at 0 h, 2 h, and 3 h at 492 nm wavelength. To perform Hoechst-PI staining, 10 μL of each dye solutions were added to the wells after 24 h of treatment. Images were obtained using fluorescence microscope with DAPI- and TRITC-filter sets. The images were analyzed *via* ImageJ software.

2.2.9. Statistical analysis. All data is presented in mean values and standard deviations of 3 independent measurements.

Student *t*-tests with Bonferroni correction were used to compare cytotoxicity between different treatments. Significance levels were determined by setting a threshold *p*-value of less than 0.05.

3. Results and discussion

3.1. Cefoperazone and tetracycline antibiotic pair solubility determination *via* HPLC

HPLC analysis was employed to determine the solubility of oppositely charged ionic antibiotic pair consisting of tetracycline hydrochloride and cefoperazone sodium salt. The retention time for tetracycline was determined to be 3.4 min, and 4.7 min for cefoperazone - see Fig. S1A and B, (SI) under the set of conditions listed in Table S1 (SI). Calibration curves were generated for each drug solution by plotting peak areas obtained by HPLC against known concentrations of antibiotics - Fig. S1C and D (SI). HLPC chromatograms of the supernatant after centrifugation of the nanocrystals of the binary antibiotic produced by mixing equimolar solutions of 4 mM sodium cefoperazone and 4 mM tetracycline hydrochloride were obtained to determine the

solubility of the antibiotic pair (Fig. S2A). The regression equation on the calibration curves was used to calculate the concentrations of tetracycline and cefoperazone dissolved in the suspension after centrifugation of nanocrystals – see Table S2 (SI). The solubility of tetracycline was calculated to be 41.43 ± 0.2 μM, and cefoperazone had a solubility of 40.06 ± 0.4 μM, see Fig. S2A (SI). This indicates that the cefoperazone and the tetracycline are in 1 : 1 ratio in the nanocrystals as the same ratio of their concentrations is found in the supernatant after the precipitation.

3.2. Zeta-potential and particle size of cefoperazone and tetracycline binary antibiotic particles stabilised with P407

P407 is shown to have a critical micelle concentration of around 0.3% (w/v) at 25 °C (equivalent to 2.6×10^{-6} M P407). The polymer in water creates micelles at concentrations exceeding this value.[45] A concentration of 0.05 wt% P407 was selected as the polymer provides steric stabilization to the formed particles of cefoperazone and tetracycline. At this concentration, P407 does not form micelles that could affect the stabilization of the antibiotic particles. The produced colloid particles were characterized by DLS and ELS using Anton Paar Litesizer 500 (particle analyzer). It was found that the non-coated NPs consisting of 2 mM tetracycline and 2 mM cefoperazone overall concentration of antibiotics, stabilized with 0.05 wt% P407 had low negative zeta-potential and exhibited particle size instability over 72 h (Fig. 2A). Particles showed gradual increase in average size from 220 nm to over 800 nm suggesting NPs aggregation over time. The particle growth leads to effectively capping the particle size due to formation of a dense P407 monolayer. Additionally, the ζ-potential of the formulation was observed to increase in absolute value over time, transitioning from nearly −4 mV to −11 mV (see Fig. 2B).

This increase in ζ-potential magnitude may be attributed to the secondary adsorption of species onto the surface of the particles, resulting in a stronger electrostatic repulsion between them. The increase in particle size with time observed in the formulation containing 1 : 1 mixture of 4 mM cefoperazone and 4 mM tetracycline in 0.05 wt% P407 can be explained by the Gibbs Thompson effect.[46]

The cationic antibiotic (tetracycline cation) and the anionic antibiotic (cefoperazone anion) interact through a combination of ionic interaction to form an electroneutral 1 : 1 complex of much lower solubility which causes precipitation. This is supported by the fact that the ratio of both antibiotics' concentrations in the supernatant which is in equilibrium with the formed particles remains practically the same as the ratio of their total concentrations (1 : 1). Hence the complex is 1 : 1, which indicates mostly ionic interactions. As Fig. 2A shows, the particle size evolves with time, mostly due to the Ostwald ripening effect due to the limited solubility of the antibiotic complex. The non-coated particles are also of low (negative) surface charge which makes them prone to further aggregation). Interestingly, the additional deposition of a coating of a cationic surfactant (HDTAB, ODTAB, DODAB) significantly impairs this process as well as leads to a surface charge reversal to moderately high positive values which provides additional repulsion. Because of their greater surface energy, smaller particles possess a tendency to dissolve whereas bigger particles tend to grow in size and form bigger crystals. The effect originates from the fact that the chemical potential of the solute at the particle interface with the solution is size-dependent and is higher at higher surface curvature (smaller particles). In the case of the non-coated formulation, settling of the particles leads to the smaller particles dissolving and mass redistribution onto the bigger particles. The accumulation of P407 on the larger particles balances the nanocrystal surface energy thus preventing further particle growth.

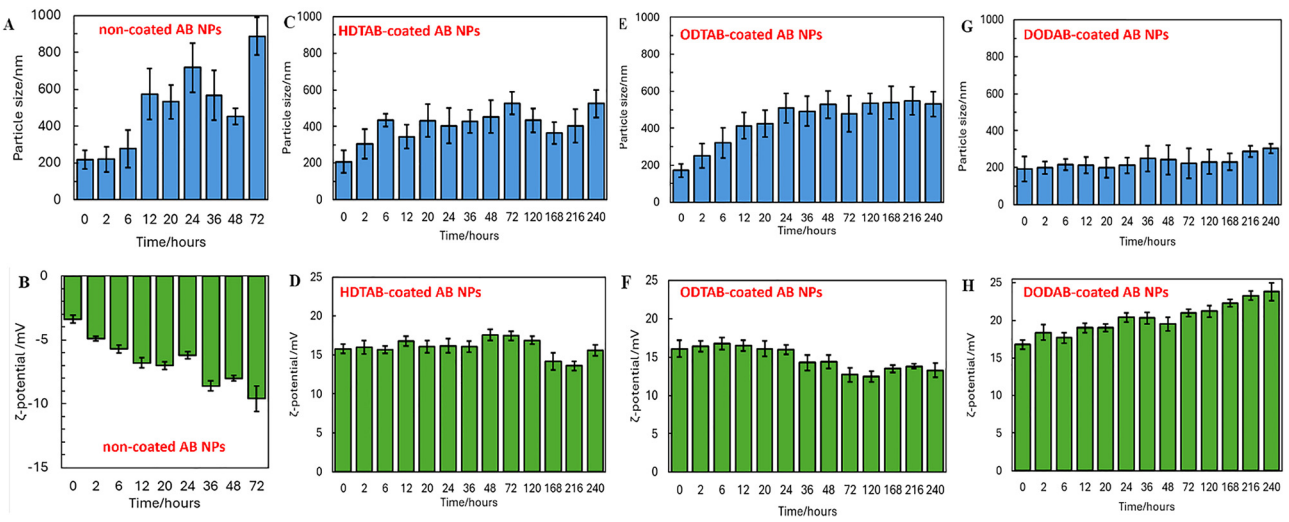

Fig. 2 (A) The mean hydrodynamic diameter and mean ζ-potential (B) of binary nanocrystals prepared by mixing in 1 : 1 ratio 4 mM cefoperazone and 4 mM tetracycline stabilised by 0.05 wt% P407 *versus* time after formulation. (C, E and D) Mean particle hydrodynamic diameter and (D, F and H) mean ζ-potentials of particle suspensions produced doping the non-coated binary antibiotic formulation of 4 mM tetracycline hydrochloride and 4 mM sodium cefoperazone at 1 : 1 ratio at 0.05 wt% P407 with ethanolic solution of 3% HDTAB (C) and (D) or (ODTAB (E) and (F) and DODAB (G) and (H) *versus* time since formulation. The particle size and the ζ-potential was monitored up to 240 hours since preparation.

3.3. Surface charge reversal of cefoperazone:tetracycline binary antibiotic particles by coating with HDTAB/ODTAB/DODAB

In order to engineer electrostatic adhesion of the formulated colloidal particles to the bacterial cell walls, the negatively charged A^+B^-NPs were doped with HDTAB/ODTAB/DODAB which are amphiphilic cationic quaternary ammonium compounds with a long hydrophobic alkyl chain. HDTAB has a very low critical micelle concentration (CMC) of 0.95 mM (0.035 wt%) while ODTAB and DODAB are practically insoluble in water. Although HDTAB as an individual agent has the ability to intercalate into the bacterial cell walls, its cytotoxicity often depends on the cell types and monomer concentration.[47] Non-coated NPs were charge-reversed by addition of very small amount of HDTAB, ODTAB and DODAB surfactants. Typically, 0.0075 wt% of cationic surfactants were used for this doping process, delivered as 3 wt% solution in ethanol to the particle suspension. The resulting three types of coated NPs were studied for particle size and zeta potential stability for over 240 hours. The stability of the HDTAB-coated NPs was analyzed in Fig. 2C showing a gradual increase in particle size over time for these HDTAB-coated binary antibiotic NPs, starting at around 200 nm and reaching approximately 400 nm by 240 h since preparation. This increase suggests that the formulation exhibits some minor aggregation over time, though it remains relatively stable over 240 h. Fig. 2D shows the ζ-potential, which stays relatively stable around +15 mV, indicating a higher level of stability and suggesting that the HDTAB-coated formulation retains its surface charge during the observed period. Since secondary adsorption of HDTAB also lowers the A^+B^-NPs surface energy this explains the slight decrease in the particle size before reaching a plateau. The decrease in the particle size of the HDTAB-coated particle formulation from approximately 400 nm to around 320 nm is noteworthy. The reversal of the surface charge of the colloidal particles results in the change of the ζ-potential increases from around −4 mV to +15 mV would allow the coated particles to adhere and accumulate on the cell walls of bacteria. In Fig. 2E and F, the stability of the particle size and ζ-potential of the formulation coated with ODTAB was monitored for 240 h. Fig. 2E shows a slight increase in particle size, but the particles remain relatively stable over time, with sizes ranging from 200 nm to 400 nm. Fig. 2F shows that ζ-potential of the ODTAB-coated binary antibiotic particle is relatively stable at the first 24 h, followed by a very slight decrease. The particle formulation coated with ODTAB shows slightly improved stability in particle size compared to HDTAB-coated binary antibiotic nanoparticle formulations. Fig. 2G demonstrates that the particle size for DODAB-coated binary antibiotic NPs remains relatively constant with slight fluctuations between 200 nm and 300 nm over a period of 240 h.

Fig. 2H shows that the ζ-potential stays within a stable range of +15 to +20 mV during the observed period, indicating that the particles surface charge remains relatively constant, and that the formulation is stable over time. The DODAB-coated particle formulation seems to be the best compromise between smaller particle size and stability. The impact of diluting of the initial formulation of 2 mM cefoperazone and 2 mM tetracycline at 0.05 wt% P407 on the particle size and ζ-potential was investigated. Fig. S3A–D (SI) shows an increase in particle size and an increase in the absolute value of ζ-potential, especially for ODTAB-coated and DODAB-coated particles. Notably, the particle size of the most diluted particle formulation, which was about 350 nm, did not exceed the size of the non-diluted formulation. The electric double layer formed around the charged particles and the ionic strength affect their ζ-potential. Moreover, the magnitude of the ζ-potential is influenced by the ionic strength, which decreases upon dilution. This reduction in the ionic strength reduces the screening effect of the ions around the particles, consequently resulting in an increase in the magnitude of the positive ζ-potential. The effect of increasing zeta potential magnitude by dilution of the binary antibiotic suspension concentration can be explained as the surfactants ODTAB and DODAB are insoluble once deposited on the particles surface (Fig. S3F and H, SI). Since the surfactant is deposited at the same overall concentration for each dilution, the higher the suspension dilution, the smaller is the number of particles produced, which accumulate the same amount of cationic surfactant upon coating. This results in a higher magnitude of the positive zeta potential of the ODTAB- or DODAB-coated particles. HDTAB has low but finite solubility and can partially desorb from the particles upon dilution, so in this case the zeta potential levels off (Fig. S3D, SI). In all three cases, however, the particles size is relatively stable (Fig. S3C, E and G, SI) with the increase of the dilution as the particle aggregation is suppressed the significant positive surface charge and the resulting electrostatic repulsion between the particles. Similar effects are reported by Galantini *et al.*[67,68] for micellar aggregates.

3.4. Electron microscopy, FTIR spectra and EDS analysis for the binary antibiotic nanoparticle formulations

The TEM images of the non-coated binary antibiotic particles formulation showed spherical morphology with the average size of 128 nm and higher (Fig. 3A). The mean diameter of the HDTAB-, ODTAB- and DODAB-coated particles determined from the TEM images (Fig. 3B, C and D) was slightly higher, 130 nm, 138 nm and 134 nm, respectively. This is likely to be the effect of drying of particles and loss of hydration water. Similar is the case from the SEM images (Fig. 3E, F, G and H), where the average particle size of non-coated, HDTAB-coated, ODTAB-coated and DODAB-coated particles were measured to be 166 nm, 165 nm, 180 nm and 204 nm, respectively. These values are consistently lower than the results from the DLS measurements (Fig. 2), most likely due to loss of hydration water upon drying. Coated binary antibiotic particle formulations show more uniform particles which indicated that the cationic surfactant coating affects the particle morphology and uniformity.

To demonstrate the presence of both antibiotics in the formulation and the HDTAB coating, EDS analysis (energy-dispersive X-ray spectroscopy) and FTIR (Fourier Transform Infrared Spectroscopy) spectra were conducted. Table S6 (SI) presents the findings of EDS analysis, including the mass% and atom% of each element for both formulations. The presence of sulfur atoms suggests the presence of cefoperazone, while the

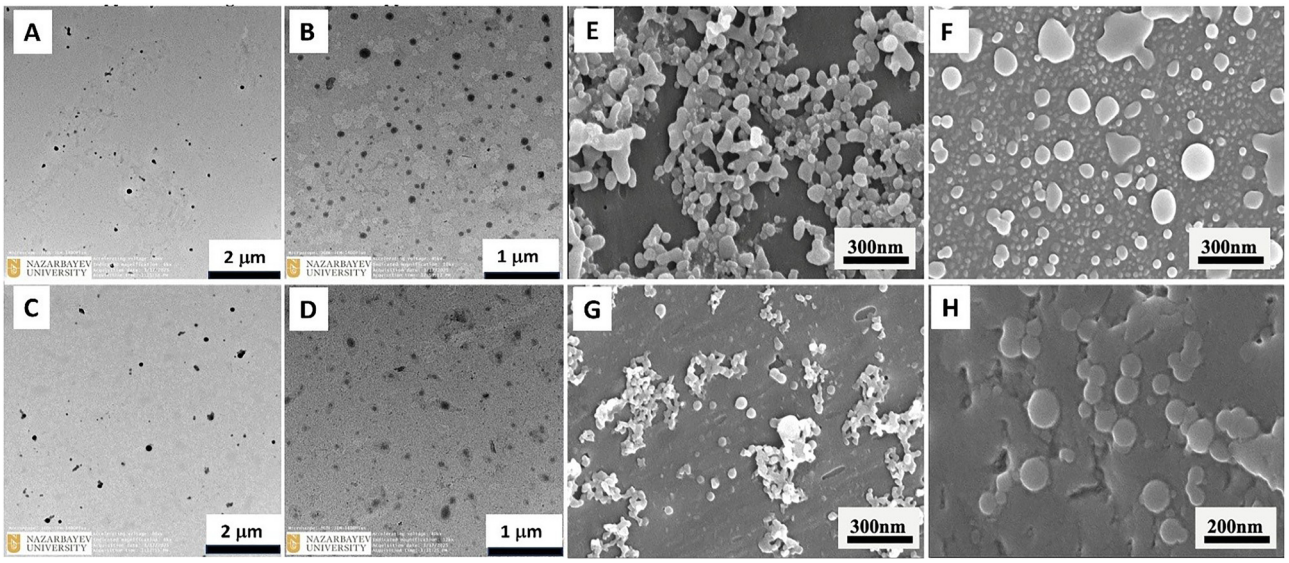

Fig. 3 (A–D) TEM images and (E–H) SEM images of the binary antibiotic particles prepared from 1 : 1 mixture of 4 mM cefoperazone and 4 mM tetracycline in 0.05 wt% P407 followed by doping with 3% ethanolic solutions of HDTAB (B) and (F), ODTAB (C) and (G) and DODAB (D) and (H). The overall concentration of cationic surfactant (HDTAB, ODTAB or DODAB) in the formulation after doping was typically 0.0075 wt%. (A) and (E) correspond to the non-coated suspension of binary antibiotic particles.

higher nitrogen content in the coated formulation indicates the presence of HDTAB coating (with non-overlapping confidence intervals for both mass% and atom%). EDS spectra for both formulations are shown in Fig. S7 (SI).

The FTIR spectra were obtained for powders of tetracycline, cefoperazone, P407, HDTAB, as well as non-coated 1 : 1 co-precipitated 4 mM cefoperazone and 4 mM tetracycline at 0.05 wt% P407 particle formulation, the same formulation coated with 0.0075 wt% HDTAB (as presented in Fig. S4 (SI)), the same formulation coated with 0.0075 wt% ODTAB (Fig. S5 (SI)), and the same formulation coated with 0.0075 wt% DODAB. Tables S3–S5 (SI) show the characteristic peaks for all three coated formulations and their constituting components. Peak broadening around 3500 cm^{-1} characteristic for cefoperazone can also be observed for the formulation, along with the peak at 1700 cm^{-1}.

The abundant C–H aliphatic stretching at 2930 cm^{-1} and 2852 cm^{-1} typical for the surfactant chains and the CH_2 group in poloxamer 407 are present in the coated formulation. The stretching of C–N abundant in both cefoperazone and tetracycline is also found in the non-coated and coated formulations. The N–H and C–H bending at aromatic C═C contributes to the transition at 1611 cm^{-1} and 1597 cm^{-1} and is present in tetracycline as well as the non-coated and coated formulations. Due to the lack of distinguishing infrared absorption bands, S–C bonds stretching occurring at 800 cm^{-1} are rarely seen in FTIR spectra as they are often overlapped by C–H bending in alkenes. Though the vibrational modes of nearby bonds can be impacted by the presence of sulfur in a molecule, this can influence the overall FTIR spectrum. For cefoperazone, the sulfur atom affects the stretching vibrations of nearby carbon–nitrogen and carbon–carbon bonds, resulting in recognizable absorption bands in the FTIR spectrum.

3.5. Electron microscopy of bacteria treated with HDTAB/ODTAB/DODAB coated binary antibiotic NPs

The SEM images of *E. coli* and *S. aureus* after incubation with the three different coated binary antibiotic suspensions confirm the attachment of all three types of coated NPs to the cell wall of bacteria (Fig. 4C–H) which can be directly seen on the cell surface in large numbers. This result is a direct proof that due to their positive surface charge, the HDTAB, ODTAB and DODAB-coated particles are electrostatically attracted to the negatively charged surface of bacterial cell wall. Note the profound change of the bacterial cell morphology compared with the non-treated bacterial samples (Fig. 4A and B). This explains the accumulation of a large amount of binary antibiotics on the cell walls of the treated bacteria and the enhancement of antibacterial action (see Fig. 5 and 6 below). TEM image of *E. coli* after 12 h of incubation with A^+B^-NPs produced from 4 mM cefoperazone and 4 mM tetracycline at 0.05 wt% P407 formulation coated with 0.0075 wt% HDTAB is shown in Fig. S8 (SI). Due to electrostatic attraction between the positively charged particles and negatively charged bacterial cell wall, the accumulation of the particles can be seen in the TEM image.

3.6. Antibiotic release profile for free antibiotics and binary antibiotic NPs *via* dialysis

We have compared the drug release profile *via* dialysis as the graphs in Fig. S2B (SI) illustrate the release rates of both free tetracycline and tetracycline from binary antibiotic NPs stabilized with P407 over a time interval of 1500 min. The release from a formulation made by co-precipitation of 4 mM : 4 mM tetracycline : cefoperazone in 0.05 wt% P407 was studied using dialysis over specified periods, allowing the analysis of how the drug concentration changes with time by HPLC. Both the free

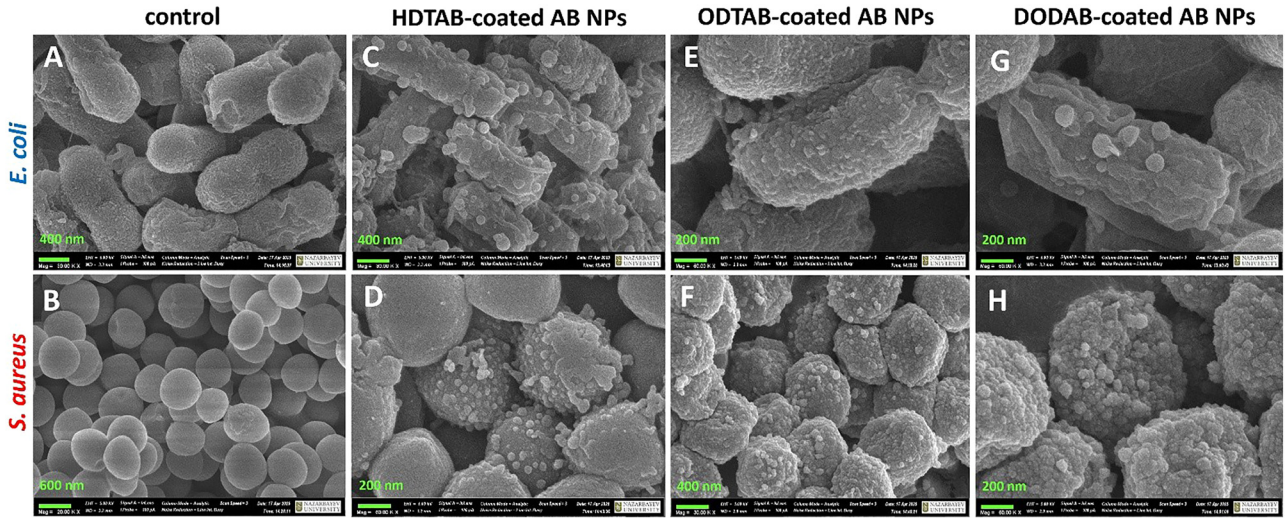

Fig. 4 SEM images (A) and (B) of the dried control samples of *E. coli* and *S. aureus* (no treatment), (C)–(H) SEM images of *E. coli* and *S. aureus* after 1.5 hours of treatment with non-coated binary antibiotic nanoparticles prepared by mixing 4 mM tetracycline and cefoperazone solutions in stabilized with 0.05 wt% P407 in 1 : 1 volume ratio, and binary antibiotic NPs coated further with HDTAB (C) and (D), ODTAB (E) and (F), and DODAB (G) and (H). The SEM images indicate different levels of bacterial membrane disruption and accumulation of NPs depending on the particle surface coating. The average particle sizes are: 136 nm for HDTAB-coated NPs; 152 nm for ODTAB-coated NPs and 114 nm for DODAB-coated NPs.

and the encapsulated antibiotics show initial rapid release, followed by a plateau as equilibrium is reached. The two curves in Fig. S2B (SI) follow with time very closely, indicating a relatively rapid dissolution of the binary antibiotic particles with the dilution of the stock suspension which allows sustained release on both antibiotics.

3.7. Antimicrobial effect of the coated and non-coated particles as well as their components on *S. aureus* and *E. coli*

Fig. 5A–D and 6A–D show the results of a 24 h time-kill assay comparing non-coated particles of overall 2 mM cefoperazone and 2 mM tetracycline stabilised with 0.05 wt% P407 and 2 mM cefoperazone and 2 mM tetracycline stabilised with 0.05 wt%

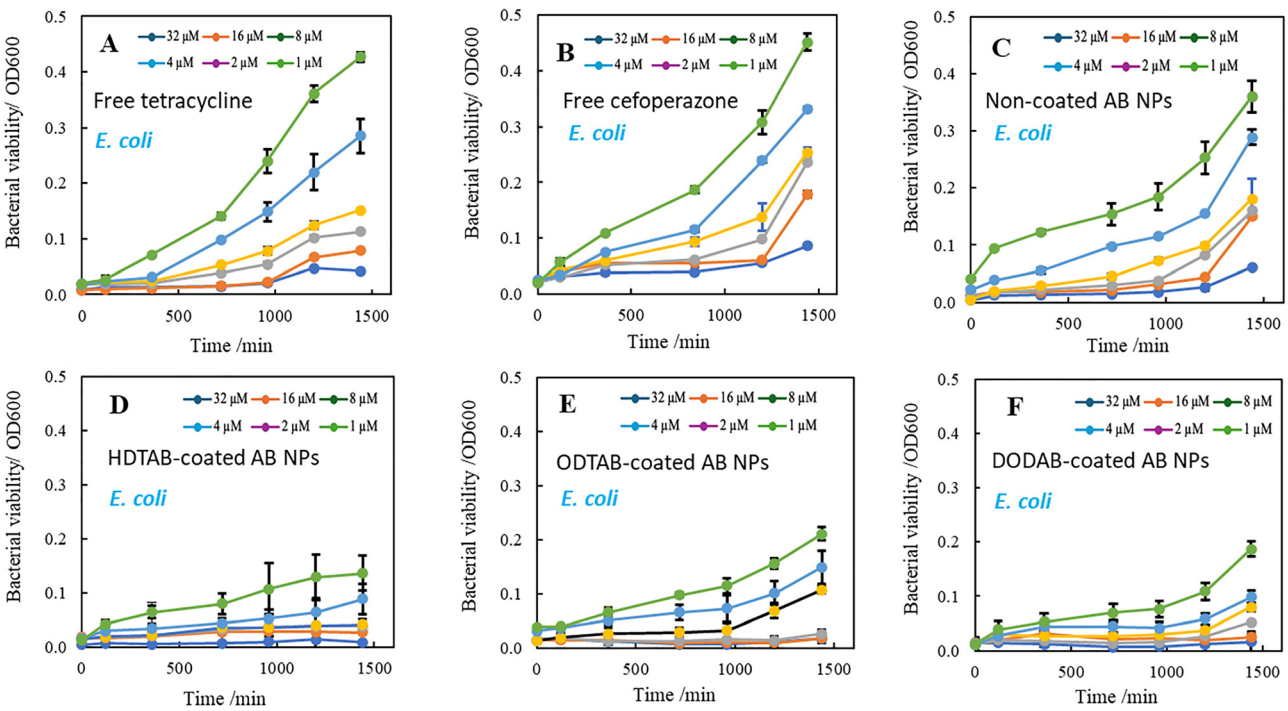

Fig. 5 Time-kill assay on *E.coli* bacteria treated with free tetracycline (A); free cefoperazone (B); as well as non-coated particles made of 4 mM cefoperazone and 4 mM tetracycline in 0.05 wt% P407 mixed in 1 : 1 volume ratio (C). Time-kill assay on *E.coli* bacteria after treatment with HDTAB-coated binary antibiotic NPs (D); ODTAB-coated binary antibiotic NPs (E) and DODAB-coated binary antibiotic NPs (F). Time-kill curves were constructed over 24 h time period, showing the impact of different concentrations (32 μM, 16 μM, 8 μM, 4 μM, 2 μM, 1 μM) of each formulation on the bacterial viability (assessed by measuring OD600).

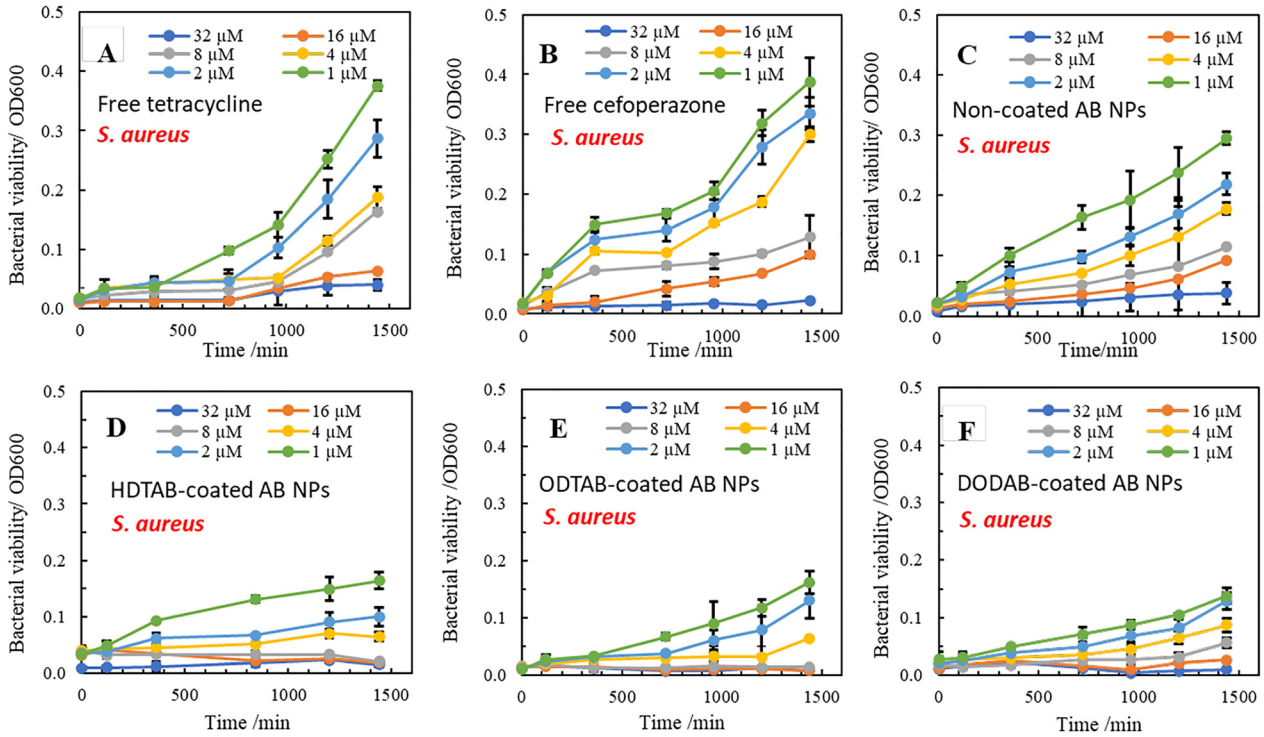

Fig. 6 Time-kill assay on *S. aureus* bacteria treated with free tetracycline (A); free cefoperazone (B); as well as non-coated particles made of 4 mM cefoperazone and 4 mM tetracycline in 0.05 wt% P407 mixed in 1 : 1 volume ratio (C). Time-kill assay on *E.coli* bacteria after treatment with HDTAB-coated binary antibiotic NPs (D); ODTAB-coated binary antibiotic NPs (E) and DODAB-coated binary antibiotic NPs (F). Time-kill curves were constructed over 24 h time period, showing the impact of different concentrations (32 μM, 16 μM, 8 μM, 4 μM, 2 μM, 1 μM) of each formulation on the bacterial viability (assessed by measuring of OD600).

P407 formulation coated with 0.0075 wt% HDTAB or ODTAB or DODAB on *E. coli* and *S. aureus.* The graphs demonstrate that the coated binary antibiotic particle formulation were more effective at reducing the bacterial growth than the free antibiotics at equivalent concentrations. The individual antibiotics exhibited significantly lower antimicrobial activity at the same overall concentrations. Similar is the case of non-coated nanoparticle formulation which also outperforms the individual antibiotics. However, the ODTAB-coated and the DODAB-coated formulations (Fig. 5E and F and 6E and F) perform more than twice better than the non-coated formulation and over trice better than the free antibiotics at equivalent low concentrations of 1 μM (Fig. 5A and B and 6A and B) for both *E. coli* and *S. aureus*, respectively. The HDTAB-coated formulation was only over twice better in suppressing bacterial growth than the free antibiotics for both types of bacteria. The data indicated that all coated particle formulations allowed to significantly improve the antimicrobial action of the individual antibiotics. Given the electrostatic adhesion of the coated particles onto both Gram-positive and Gram-negative bacteria, the local concentration of the antibiotic is significantly increased leading to the enhancement of the antibiotic properties. However, at high overall concentrations (32 μM), the HDTAB-coated formulations seem to perform better than ODTAB- and DODAB-coated formulation. Note that the cationic surfactant overall concentration effectively increases with the increase of the antibiotic concentration as all dilutions are made from the same stock solution. The antimicrobial activity was also studied after incubating *E. coli* and *S. aureus* for 24 h with of tetracycline, cefoperazone, as well as particles obtained by 1 : 1 mixing of 4 mM cefoperazone and 4 mM tetracycline stabilized with 0.05 wt% P407 coated with HDTAB, ODTAB or DODAB (Fig. 7A and B). This result is consistent with the findings in Fig. S3D, F and H (SI), which investigated the effect of dilution on the particle surface charge. One can see that the positive zeta-potential increases upon dilution for both ODTAB-coated and DODAB-coated particles while it stays constant for HDTAB-coated binary antibiotic particles. Due to their positive surface charge, the HDTAB/ODTAB/DODAB-coated binary antibiotic particles are accumulated on the bacterial cell wall, delivering very high local concentration of both antibiotics which is more effective in killing both types of bacteria. However, there is no evidence that these particles directly penetrate the bacterial cells walls (see *e.g.* Fig. S8, SI). This is contrasted by the zeta potential of the non-coated particles which stays around zero for the applied dilutions and explains why the antimicrobial activity of the coated particles is so much better than those of the free antibiotics and the non-coated particles. The latter is supported by the SEM images of both *E. coli* shown in Fig. 4C, E and G and *S. aureus* shown in Fig. 4D, F and H after incubation with binary antibiotic particles coated with HDTAB or ODTAB or DODAB. Similar effect is demonstrated in Fig. S8 (SI) on TEM of *E.coli* isolated after incubation with HDTAB-coated binary antibiotic particles.

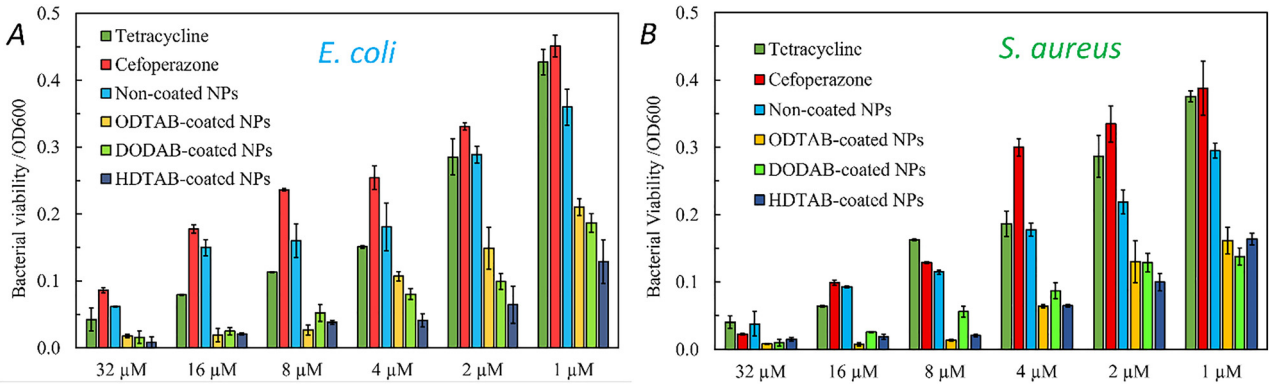

Fig. 7 The relative cell viability of (A) *E. coli* (B) *S. aureus* and upon 24-hour incubation with various formulations as 2 mM free tetracycline hydrochloride, 2 mM free sodium cefoperazone, as well as binary antibiotic particles containing 2 mM cefoperazone and 2 mM tetracycline stabilised with 0.05 wt% P407 and the same coated particles with 0.0075 wt% HDTAB or ODTAB or DODAB at the same conditions. All formulations were mixed with the bacterial broth to reach the targeted antibiotic concentration for each treatment.

3.8. Cytotoxicity of the coated and non-coated binary antibiotic particle formulations as well as their constituents on human cells

Fig. 8A shows the results of MTS cell proliferation assay performed with human cell line HaCaT as a convenient proxy for human keratinocyte cells. MTS is a water-soluble tetrazolium salt used to assess the metabolic activity of cells, providing information on cell viability and proliferation ability. In living cells MTS (which has yellow color) is converted to a water-soluble purple formazan product by mitochondrial enzymes.

A higher number of viable cells can convert a fixed concentration of MTS into a higher amount of formazan, which is proportional to the number of viable cells but it also depends on their metabolic activity. The MTS assay is often used to evaluate cell proliferation ability upon exposure to various therapies, drug formulations and different treatments. The concentrations of all treatments were kept the same as those in the final particle formulation from mixing 1 : 1 of 4 mM cefoperazone and 4 mM tetracycline stabilized with 0.05 wt% P407 and coated with HDTAB or ODTAB or DODAB. Cell proliferation is represented in percentage relative to the control (no treatment) for P407, free antibiotics and non-coated particle formulation which all showed very small effect on the cell's proliferation. However, HDTAB-coated formulation demonstrated a reduction in the cell proliferation probably due to the finite solubility of HDTAB. This stagnation in the cell proliferation is likely due to the

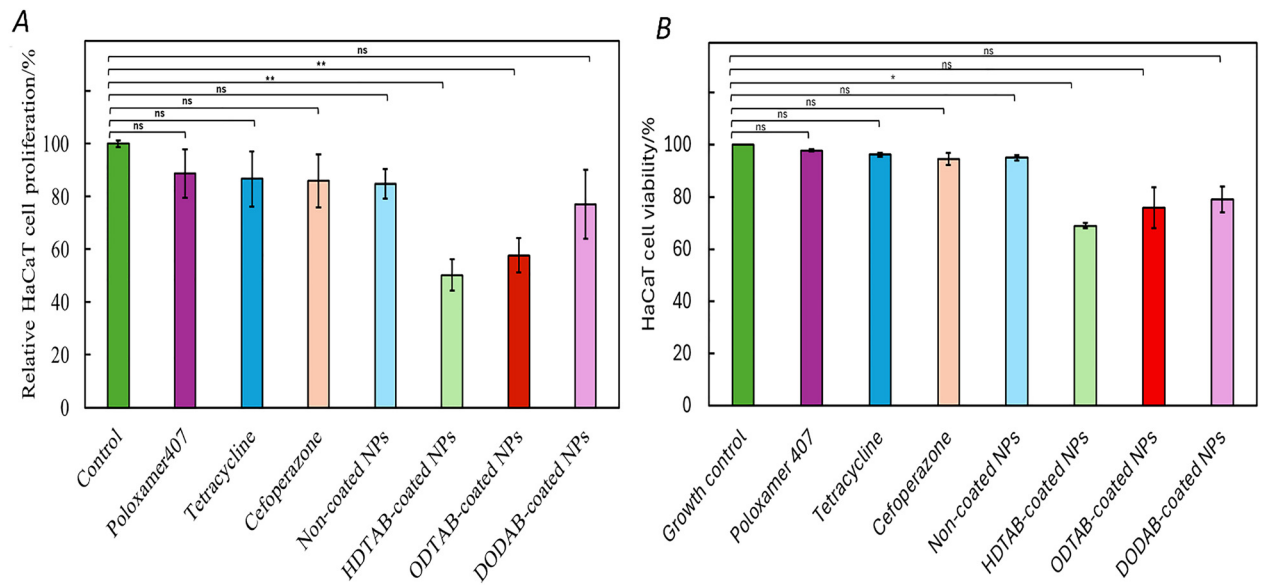

Fig. 8 Cytotoxicity upon incubation of HaCaT cells with formulations of 0.05 wt% solution P407, 2 mM free tetracycline hydrochloride, 2 mM free sodium cefoperazone, as well as binary antibiotic particles produced by mixing 4 mM cefoperazone and 4 mM tetracycline stabilised with 0.05 wt% P407 formulation and coated binary antibiotic particles obtained from 4 mM cefoperazone and 4 mM tetracycline stabilised with 0.05 wt% P407 coated further with 0.0075% HDTAB, or 0.0075% ODTAB or 0.0075% DODAB. The cell proliferation (A) was assessed after 24 h of each treatment by using the MTS assay on HaCaT cell line. The cell viability (B) was assessed after 24 h on HaCaT cells by using Hoechst/PI staining using fluorescence microscopy and image analysis.

presence of low concentrations of desorbed HDTAB, which is known for its ability to disrupt cell membranes, as previously discussed since non-coated particles showed 50% cell proliferation compared to the control. Lower effects on the cell proliferation were observed for ODTAB-coated formulation and very small for DODAB-coated formulation on the cell proliferation which is also linked to their insolubility in water.

To further examine the cytotoxicity of the formulation and its constituents, propidium iodide (PI) and Hoechst fluorescent dyes were employed in a double staining procedure after the 24 h treatment of the HaCaT cells with the particle formulations of coated and non-coated binary antibiotic particles, respectively, as shown in Fig. 8B. These dyes are commonly used to detect both the total number of cells present in a sample (Hoechst staining), as well as the number of dead cells (PI staining), allowing for a comprehensive assessment of cytotoxicity. PI only enters cells with damaged cell membranes and intercalates within the DNA. Then, it becomes fluorescent upon excitation with 500 nm light and emits red fluorescence of 617 nm. Hoechst penetrating intact cells also bind to DNA and emit blue fluorescence when excited by light of 360 nm wavelength with emitted light of 460 nm wavelength - see Fig. S9 (SI). The results of PI and Hoechst staining showed that after 24 h treatment with the non-coated formulation, over 91% of HaCaT cells remained viable. However, treatment with the coated formulation resulted in a lower percentage of viable HaCaT cells, 67% for HDTAB-coated, 76% for ODTAB-coated and over 80% for DODAB-coated particles. These findings confirm the marginal cytotoxic effects of the ODTAB- and DODTAB-coated formulations and the moderate cytotoxicity of the HDTAB-coated formulation after 24 h of treatment.

4. Conclusions

We developed a new concept of binary antibiotic nanoparticles prepared by co-precipitation of a cationic and an anionic antibiotic in the presence of surface-active polymer (Pluronic surfactant P407) in aqueous solution. Specifically, novel binary antibiotic nano-formulation consisted of tetracycline-cefoperazone cores sterically stabilized with P407 and further coated with a cationic surfactant. The major advantages of these antibiotic nanocarriers are that they: (i) amplify the antimicrobial effect of the two individual antibiotics and (ii) do not leave a nanomaterials post-use as their cores dissolve. The cationic surface functionality of the binary antibiotic nanoparticles allows them to adhere to the negatively charged bacterial cell wall which enhances their antimicrobial efficacy against both Gram-negative and Gram-positive bacteria, represented as *E. coli* and *S. aureus*, respectively. It was found that the formulation with ODTAB and DODAB surface functionalisation perform better than the one coated with HDTAB. The developed formulation reduces the overall concentration of the antibiotics needed to eliminate the bacteria compared to application of free individual antibiotics. This can potentially allow for reduction of the therapeutic dosage and/or increase of the antimicrobial efficiency. The employment of the negligible amounts of biocompatible surface-active polymer for steric stabilization as well as doping with an (insoluble) cationic surfactant may allow these formulations to be developed as intravenous therapy or oral delivery as the particles would dissolve with time without leaving residual nanocarriers. In conclusion, the binary antibiotic nanoparticle created in this study offers a viable solution for the problem of increasing bacterial antibiotic tolerance. This discovery lays the groundwork for future investigations into the development of safe and effective formulations for the treatment of bacterial infections and tackling AMR.

Author contributions

V. N. P. gave the idea of the project and the methodology, secured the funding, and supervised the whole research team. He edited the final draft of the manuscript. N. N., A. K. and Y. K. did experiments on the binary antibiotic nanoparticles' preparation and characterisation, figures preparation and contributed to draft writing. N. N. also contributed with testing their amicrobial action on *E. coli* and *S. aureus* and their cytotoxicity on HaCaT cells along with the data analysis. A. K. F. D. provided technical help and student supervision. The final version of the manuscript was approved by all authors.

Conflicts of interest

There are no conflicts to declare.

Data availability

All data regarding this manuscript are already presented in the graphs of the main paper and the supplementary information (SI) file. Supplementary information: in the enclosed SI we present the following additional data: (i) method conditions for HPLC analysis of cefoperazone and tetracycline; (ii) HPLC chromatograms of sodium cefoperazone, tetracycline hydrochloride and calibration graphs for quantitative analysis; (iii) the mean concentrations of the soluble antibiotics in the binary antibiotic particle suspension are found *via* HPLC and the AB NPs release kinetics from dialysis; (iv) effect of the dilution on the particles size and zeta potential of the non-coated and HDTAB-, ODTAB- or DODAB-coated binary antibiotic particles; (v) FTIR spectra for tetracycline, cefoperazone, Poloxamer 407, HDTAB, and the HDTAB-coated binary antibiotic particles; (vi) FTIR spectra for tetracycline, cefoperazone, Poloxamer 407, ODTAB, and the ODTAB-coated binary antibiotic particles; (vii) FTIR spectra for tetracycline, cefoperazone, Poloxamer 407, DODAB, and the DODAB-coated binary antibiotic particles; (viii) tabulated FTIR peaks for HDTAB-, ODTAB- and DODAB coated and non-coated NPs (ix) EDS diagram of the non-coated and HDTAB-coated binary antibiotic particles; (x) tabulated EDS analysis results of HDTAB-coated and non-coated A+B-NPs; (xi) TEM image of *E. coli* after incubation with HDTAB-coated binary antibiotic particles; (xii) HaCaT cells after 24 h of incubation with complete media without treatment, with non-coated and

HDTAB-, ODTAB- or DODAB-coated binary antibiotic particle suspension. See DOI: https://doi.org/10.1039/d5ma01493j.

Acknowledgements

V. N. P. acknowledges funding from his Faculty Development Competitive Research Grant (Grant 040225FD4704, V. N. P.) of Nazarbayev University. Y. K. and N. N. thank Nazarbayev University for the financial support of their MSc thesis and BSc honours studies. The authors thank Issayev Zhanpeis, the HPLC operator from NU Core Research Facilities, for his expert technical assistance. All authors thank Drs Ellina Mun and Timur Atabaev at NU for taking the time to review this work and offer constructive criticism and valuable suggestions.

Notes and references

1 B. Tornimbene, S. Eremin, M. Escher, J. Griskeviciene, S. Manglani and C. L. Pessoa-Silva, *Lancet Infect. Dis.*, 2018, **18**, 241–242.
2 M. A. Kohanski, D. J. Dwyer and J. J. Collins, *Nat. Rev. Microbiol.*, 2010, **8**, 423–435.
3 S. Wang, Y. Gao, Q. Jin and J. Ji, *Biomater. Sci.*, 2020, **8**, 6825–6839.
4 J. M. V. Makabenta, A. Nabawy, C. H. Li, S. Schmidt-Malan, R. Patel and V. M. Rotello, *Nat. Rev. Microbiol.*, 2021, **19**, 23–36.
5 E. D. Brown and G. D. Wright, *Nature*, 2016, **529**, 336–343.
6 D. K. Singh, J. Kumar, V. K. Sharma, S. K. Verma, A. Singh, P. Kumari and R. N. Kharwar, *Nanomedicine*, 2017, **13**, 191–207.
7 G. Mi, D. Shi, M. Wang and T. J. Webster, *Adv. Healthcare Mater.*, 2018, **7**, e1800103.
8 S. C. T. Moorcroft, D. G. Jayne, S. D. Evans and Z. Y. Ong, *Macromol. Biosci.*, 2018, **18**, 1800207.
9 S. Baek, S. H. Joo and M. Toborek, *J. Hazard. Mater.*, 2019, **373**, 122–130.
10 A. Baranwal, A. Srivastava, P. Kumar, V. K. Bajpai, P. K. Maurya and P. Chandra, *Front. Microbiol.*, 2018, **9**, 422.
11 P. Makvandi, C. Yu Wang, E. N. Zare, A. Borzacchiello, L. Na Niu and F. R. Tay, *Adv. Funct. Mater.*, 2020, **30**, 1910021.
12 S. E. Birk, A. Boisen and L. H. Nielsen, *Adv. Drug Delivery Rev.*, 2021, **174**, 30–52.
13 H. Soria-Carrera, A. Lucía, L. De Matteis, J. A. Aínsa, J. M. de la Fuente and R. Martín-Rapún, *Macromol. Biosci.*, 2019, **19**, 1970012.
14 S. S. M. Al-Obaidy, A. F. Halbus, G. M. Greenway and V. N. Paunov, *J. Mater. Chem. B*, 2019, **7**, 3119–3133.
15 P. J. Weldrick, S. San and V. N. Paunov, Advanced Alcalase-Coated Clindamycin-Loaded Carbopol Nanogels for Removal of Persistent Bacterial Biofilms, *ACS Appl. Nano Mater.*, 2021, **4**, 1187–1201.
16 K. Forier, K. Raemdonck, S. C. De Smedt, J. Demeester, T. Coenye and K. Braeckmans, *J. Controlled Release*, 2014, **190**, 607–623.
17 H. A. Hemeg, *Int. J. Nanomed.*, 2017, **12**, 8211–8225.
18 S. Muzammil, S. Hayat, M. Fakhar-e-Alam, B. Aslam, M. H. Siddique, M. A. Nisar, M. Saqalein, M. Atif, A. Sarwar, A. Khurshid, N. Amin and Z. Wang, *Front. Biosci., Elite Ed.*, 2018, **10**, 352–374.
19 H. Jahangirian, E. G. Lemraski, T. J. Webster, R. Rafiee-Moghaddam and Y. Abdollahi, *Int. J. Nanomed.*, 2017, **12**, 2957–2978.
20 A. Fakhri, S. Tahami and M. Naji, *J. Photochem. Photobiol. B Biol.*, 2017, **169**, 21–26.
21 D. Lomelí-Marroquín, D. M. Cruz, A. Nieto-Argüello, A. V. Crua, J. Chen, A. Torres-Castro, T. J. Webster and J. L. Cholula-Díaz, *Int. J. Nanomed.*, 2019, **14**, 2171–2190.
22 B. Rao and R. C. Tang, *Adv. Nat. Sci.: Nanosci. Nanotechnol.*, 2017, **8**, 015014.
23 S. J. Nadaf, S. A. Bandgar, I. D. Raut, S. V. Patil, S. G. Killedar and S. S. Patil, *Nanoscale Processing*, Elsevier, 2021, pp. 361–382.
24 M. Azizi-Lalabadi, A. Ehsani, B. Divband and M. Alizadeh-Sani, *Sci. Rep.*, 2019, **9**, 17439.
25 J. M. Munita and C. A. Arias, Mechanisms of Antibiotic Resistance, *Microbiol. Spectrum*, 2016, **4**, 0016–2015, DOI: 10.1128/microbiolspec.VMBF-0016-2015VMBF-.
26 A. Zhivich, *Microbiol. Indep. Res.*, 2017, **4**, 31–51.
27 H. A. Hemeg, *Int. J. Nanomed.*, 2017, **12**, 8211–8225.
28 J. T. Seil and T. J. Webster, *Int. J. Nanomed.*, 2012, **7**, 2767–2781.
29 A. F. Halbus, T. S. Horozov and V. N. Paunov, *Adv. Colloid Interface Sci.*, 2017, **249**, 134–148.
30 J. Rodríguez-Beltrán, J. DelaFuente, R. León-Sampedro, R. C. MacLean and Á. San Millán, *Nat. Rev. Microbiol.*, 2021, **19**, 347–359.
31 I. L. Brito, *Nat. Rev. Microbiol.*, 2021, **19**, 442–453.
32 P. J. Weldrick, A. Wang, A. F. Halbus and V. N. Paunov, Emerging nanotechnologies for targeting antimicrobial resistance, *Nanoscale*, 2022, **14**, 4018–4041.
33 J. Kim, J. S. Hahn, M. J. Franklin, P. S. Stewart and J. Yoon, *J. Antimicrob. Chemother.*, 2009, **63**, 129–135.
34 B. S. Tseng, W. Zhang, J. J. Harrison, T. P. Quach, J. L. Song, J. Penterman, P. K. Singh, D. L. Chopp, A. I. Packman and M. R. Parsek, *Environ. Microbiol.*, 2013, **15**, 2865–2878.
35 F. Nederberg, Y. Zhang, J. P. K. Tan, K. Xu, H. Wang, C. Yang, S. Gao, X. D. Guo, K. Fukushima, L. Li, J. L. Hedrick and Y. Y. Yang, *Nat. Chem.*, 2011, **3**, 409–414.
36 R. F. Landis, C. H. Li, A. Gupta, Y. W. Lee, M. Yazdani, N. Ngernyuang, I. Altinbasak, S. Mansoor, M. A. S. Khichi, A. Sanyal and V. M. Rotello, *J. Am. Chem. Soc.*, 2018, **140**, 6176–6182.
37 A. F. Radovic-Moreno, T. K. Lu, V. A. Puscasu, C. J. Yoon, R. Langer and O. C. Farokhzad, *ACS Nano*, 2012, **6**, 4279–4287.
38 L. Liu, K. Xu, H. Wang, P. K. Jeremy Tan, W. Fan, S. S. Venkatraman, L. Li and Y. Y. Yang, *Nat. Nanotechnol.*, 2009, **4**, 457–463.
39 B. A. Nevius, Y. P. Chen, J. L. Ferry and A. W. Decho, *Ecotoxicology*, 2012, **21**, 2205–2213.
40 S. Pal, Y. K. Tak and J. M. Song, *Appl. Environ. Microbiol.*, 2007, **73**, 1712–1720.

41 P. J. Weldrick, S. Iveson, M. J. Hardman and V. N. Paunov, *Nanoscale*, 2019, **11**, 10472–10485.
42 G. Zu, M. Steinmüller, D. Keskin, H. C. Van Der Mei, O. Mergel and P. Van Rijn, *ACS Appl. Polym. Mater.*, 2020, **2**, 5779–5789.
43 Y. Liu, H. J. Busscher, B. Zhao, Y. Li, Z. Zhang, H. C. Van Der Mei, Y. Ren and L. Shi, *ACS Nano*, 2016, **10**, 4779–4789.
44 Y. Liu, Y. Ren, Y. Li, L. Su, Y. Zhang, F. Huang, J. Liu, J. Liu, T. G. van Kooten, Y. An, L. Shi, H. C. van der Mei and H. J. Busscher, *Acta Biomater.*, 2018, **79**, 331–343.
45 E. Giuliano, D. Paolino, M. Fresta and D. Cosco, *Medicines*, 2019, **6**, 7, DOI: 10.3390/medicines6010007.
46 L. Makkonen, *Langmuir*, 2002, **18**, 1445–1448.
47 S. Munguía-Moreno, G. A. Martínez-Castañón, N. Patiño-Marín, C. Cabral-Romero and N. V. Zavala-Alonso, *J. Nanomater.*, 2018, **2018**, 6401747.
48 S. S. M. Al-Obaidy, G. M. Greenway and V. N. Paunov, *Nanoscale Adv.*, 2019, **1**, 858–872.
49 P. J. Weldrick, M. J. Hardman and V. N. Paunov, Smart active antibiotic nanocarriers with protease surface functionality can overcome biofilms of resistant bacteria, *Mater. Chem. Front.*, 2021, **5**, 961–972.
50 M. J. Al-Awady, P. J. Weldrick, M. J. Hardman, G. M. Greenway and V. N. Paunov, Amplified antimicrobial action of chlorhexidine encapsulated in PDAC-functionalized acrylate copolymer nanogel carriers, *Mater. Chem. Front.*, 2018, **2**, 2032–2044.
51 P. J. Weldrick, S. Iveson, M. J. Hardman and V. N. Paunov, Breathing new life into old antibiotics: Overcoming antibacterial resistance by antibiotic-loaded nanogel carriers with cationic surface functionality, *Nanoscale*, 2019, **11**, 10472–10485.
52 E. O. Asare, E. A. Mun, E. Marsili and V. N. Paunov, Nanotechnologies for control of pathogenic microbial biofilms, *J. Mater. Chem. B*, 2022, **10**, 5129–5153.
53 E. O. Asare, A. Seidakhanova, D. Amangeldinova, E. Marsili and V. N. Paunov, Targeting S. epidermidis Biofilms by the Tetracycline-Loaded Nanogel Surface Functionalized with Savinase, DNase, and Cellulase, *ACS Appl. Nano Mater.*, 2023, **6**, 22792–22806.
54 M. S. Butler and D. L. Paterson, Antibiotics in the Clinical Pipeline in October 2019, *J. Antibiot.*, 2020, **73**, 329–364.
55 C. Llor and L. Bjerrum, Antimicrobial resistance: risk associated with antibiotic overuse and initiatives to reduce the problem, *Ther. Adv. Drug Saf.*, 2014, **5**, 229–241.
56 L. L. Silver, Challenges of antibacterial discovery, *Clin. Microbiol. Rev.*, 2011, **24**, 71–109.
57 S. Doron and L. E. Davidson, Antimicrobial stewardship, *Mayo Clin. Proc.*, 2011, **86**, 1113–1123.
58 P. J. Weldrick, M. J. Hardman and V. N. Paunov, Enhanced Clearing of Wound-Related Pathogenic Bacterial Biofilms Using Protease-Functionalized Antibiotic Nanocarriers, *ACS Appl. Mater. Interfaces*, 2019, **11**, 43902–43919.
59 A. Wang, P. J. Weldrick, L. A. Madden and V. N. Paunov, Biofilm-Infected Human Clusteroid Three-Dimensional Co-culture Platform to Replace Animal Models in Testing Antimicrobial Nanotechnologies, *ACS Appl. Mater. Interfaces*, 2021, **13**, 22182–22194.
60 A. F. Halbus, T. S. Horozov and V. N. Paunov, Surface-Modified Zinc Oxide Nanoparticles for Antialgal and Anti-yeast Applications, *ACS Appl. Nano Mater.*, 2020, **3**, 440–451.
61 A. F. Halbus, T. S. Horozov and V. N. Paunov, Controlling the antimicrobial action of surface modified magnesium hydroxide nanoparticles, *Biomimetics*, 2019, **4**, 41.
62 A. F. Halbus, T. S. Horozov and V. N. Paunov, Strongly Enhanced Antibacterial Action of Copper Oxide Nanoparticles with Boronic Acid Surface Functionality, *ACS Appl. Mater. Interfaces*, 2019, **11**, 12232–12243.
63 A. F. Halbus, T. S. Horozov and V. N. Paunov, Self-grafting copper oxide nanoparticles show a strong enhancement of their anti-algal and anti-yeast action, *Nanoscale Adv.*, 2019, **1**, 2323–2336.
64 M. J. Al-Awady, G. M. Greenway and V. N. Paunov, Nanotoxicity of polyelectrolyte-functionalized titania nanoparticles towards microalgae and yeast: role of the particle concentration, size and surface charge, *RSC Adv.*, 2015, **5**, 37044–37059.
65 A. P. Richter, J. S. Brown, B. Bharti, A. Wang, S. Gangwal, K. Houck, E. A. Cohen Hubal, V. N. Paunov, S. D. Stoyanov and O. D. Velev, An environmentally benign antimicrobial nanoparticle based on a silver-infused lignin core, *Nat. Nanotechnol.*, 2015, **10**, 817–823.
66 S. S. M. Al-Obaidy, G. M. Greenway, S. Kalmagambetova and V. N. Paunov, Dual surface functionalised curcumin-shellac nano-delivery system with enhanced antimicrobial action, *RSC Adv.*, 2025, **15**, 25497–25509.
67 A. A. D'Archivio, L. Galantini and E. Tettamanti, Study on Intermicellar Interactions and Micellar Size in Aqueous Solutions of Sodium Taurocholate by Measurements of Collective Diffusion and Self-Diffusion Coefficients, *J. Phys. Chem. B*, 2000, **104**, 9255–9259.
68 L. Galantini, S. M. Giampaolo, L. Mannina, N. V. Pavel and S. Viel, Study of Intermicellar Interactions and Micellar Sizes in Ionic Micelle Solutions by Comparing Collective Diffusion and Self-Diffusion Coefficients, *J. Phys. Chem. B*, 2004, **108**, 4799–4805.